Published in final edited form as:
Photochem Photobiol. 2014 ; 90(2): 402–414. doi:10.1111/php.12203.

A Spectroscopic and Theoretical Investigation of a Free-Base *meso*-Trithienylcorrole†

Jordan A. Greco[1], **Alison Rossi**[1], **Robert R. Birge**[1,2,*], and **Christian Brückner**[1,*]

[1]Department of Chemistry, University of Connecticut, Storrs, Connecticut 06269-3060 USA

[2]Department of Molecular and Cell Biology, University of Connecticut, Storrs, Connecticut 06269-3125 USA

Abstract

The unique optical properties of free-base *meso*-trithienylcorrole were compared to those of the widely investigated *meso*-triphenyl-substituted analogue. A combination of spectroscopic and computational experiments were undertaken to elucidate the relationship between structural features of the neutral, mono-anionic, and mono-cationic forms of the corroles and their corresponding optical properties. A general bathochromic shift was measured for the thienyl-substituted corrole. The experimental spectra are supported by excited state calculations. A systematic series of ground state minimizations were performed to determine energy minima for the flexible and solvent-sensitive molecules. Trithienylcorrole was found to have a more non-planar macrocycle in conjunction with a high degree of π-overlap with the *meso*-substituents. Both structural features contribute to their bathochromically shifted optical spectra. The configurational character of the thienyl-substituted corrole is shown to have a larger degree of molecular orbital mixing and doubly excited character, which suggest a more complex electronic structure that does not fully adhere to the Gouterman four-orbital model. The reactivity of the thienyl groups, particularly with respect to their ability to be (electro)-polymerized, combined with the tight coupling of the *meso*-thienyl groups with the corrole chromophore elucidated in this work, recommends the *meso*-thienylcorroles as building blocks in, for instance, organic semiconductor devices.

INTRODUCTION

The fundamental understanding of the properties of tetrapyrrolic macrocycles, the ‘pigments of life’ (1), has long been of interest for their biological significance and potential for applications in a wide variety of biological and technical applications. In an upshot of these studies, novel synthetic pathways and the discovery of many tetrapyrrolic pigments and analogues without natural precedent provided the ability to modulate the electronic structure of the porphyrinoids (2-9), an important prerequisite for the optimal utilization of these chromophores.

†This paper is part of the Special Issue honoring the memory of Nicholas J. Turro

*Corresponding author emails: rbirge@uconn.edu (Robert R. Birge) and c.bruckner@uconn.edu (Christian Brückner).

SUPPLEMENTARY MATERIALS
Table S1, S2 and S3 and Figures S1, S2 and S3 can be found at DOI: 10.1562/2006-xxxxxx.s1.

Corroles are tetrapyrrolic macrocycles that contain three methine bridges and one direct pyrrole-pyrrole bond (10). Thus, they lack one *meso*-position compared to a regular porphyrin structure (Scheme 1). However, both porphyrins and corroles contain 18 π-electron systems (with two or one 'cross-conjugated' β,β'-double bonds, respectively).

The 18 π-electron system in the contracted molecular framework of corroles is maintained by change of the hybridization state of one nitrogen. Thus, only a single imine-type nitrogen and three pyrrole-type nitrogens line the central cavity of corroles as compared to two nitrogens of each type in porphyrins.

meso-Triaryl-substituted corroles were firstly described by Gross and co-workers in 1999 (11, 12). Their syntheses were improved since (13-16, 10), and numerous investigations illuminated the unique structural and electronic aspects of triarylcorroles (and their metal complexes) (17-34). As a consequence, the smaller trianionic corrolato ligand has a greater ability to stabilize higher central metal oxidation states than the larger dianionic porphyrinato ligand (35-37). This property was utilized in applications of metallocorroles as catalysts for a range of transformations (38-44). *meso*-Arylcorroles were also utilized (45, 10, 46), *inter alia*, in light-harvesting devices (47), as chemosensors (48), and as chemotherapeutics (49-54).

With notable exceptions (55, 56), substituents attached to the *meso*-phenyl groups on porphyrins have generally only minimal influence on the electronic structure of a porphyrin (57) because the phenyl moieties are, due to an unfavorable β-H to *o*-H steric interaction, positioned essentially orthogonal to the porphyrinic chromophore (58). However, we have demonstrated that the smaller *meso*-thienyl groups lacking an *o*-H group have a pronounced influence on the conformation and electronic spectra of the porphyrinic chromophore, particularly when protonation induces a non-planar conformation of the macrocycle (59). As a result, a significant bathochromic shift of the optical spectra is observed for *meso*-thienyl-substituted porphyrins when compared to the phenyl analogues (59-64). *meso*-Thienyl-substituted porphyrins have been used in the study of rotational barriers in peripherally crowded porphyrins (65), and have been incorporated in the design of organic semiconductor devices (66), light harvesting and energy-transfer molecules (67, 68, 64), and supramolecular architectures with extended electronic states (69). *meso*-Thienyl-substituted porphyrin analogues were also reported (70, 71). Some *meso*thienyl substituted core-modified porphyrins proved to be potent phototoxins (71). Significantly, the thienyl substituents can be (electro)-polymerized to furnish, for instance, ultrathin films of quasi two-dimensional porphyrin polymers (66, 72, 73), to produce electrodes possessing electrocatalytic properties for the four-electron reduction of oxygen (74) or to be part of electrochemical glucose (75) or novel TNT sensors (76).

Because of their larger degree of non-planarity and contracted frameworks, *meso*-aryl-substituted corroles exhibit a reduced β-H to *o*-H steric interaction with their *meso*-substituents (11). Thus, the conformation of the aryl substituents can be more co-planar with the corrole chromophore than the same *meso*-substituents with the porphyrin chromophore. Consequently, this leads to a larger π-overlap with the *meso*-aryl substituents, and variation of these substituents allows a much more prominent spectral tuning of the corrole

chromophore (and its metal complexes) than is observed in comparable porphyrins (12, 77-81, 28, 26).

The group of Churchill pioneered the synthesis of *meso*-thienyl-substituted corroles and their building blocks, and studied their characteristics (82, 80, 83, 81). Through these investigations, it became clear that the presence of the *meso*-thienyl-substituents in corroles (and dipyrrin-based chromophores, such as boron-dipyrromethene (BODIPY)) (84-89) have a significant effect on the electronic structure and photophysical properties of the chromophores. However, we are not aware of a detailed description of the nature of the electronic interactions between the thienyl moieties and the central corrole chromophore.

In this contribution, we will compare the UV-visible spectra of a *meso*-tris(5-methylthien-2-yl-substituted) corrole in a number of solvents and at varying protonation/deprotonation states with the corresponding spectra of its triphenyl-substituted analogue. This investigation assesses the degree to which the thienyl groups influence the optical spectra of free-base thienylcorroles. Moreover, a computational study will delineate structural implications of the electronic overlap of the two π-systems and will define the origins of the observed differences between a *meso*-phenyl- and *meso*-thienyl-substituted corrole. We thus provide complementary information to the existing studies that describe the often surprising electronic properties of corroles.

METHODS AND MATERIALS

Materials

All reagents and solvents were from commercial sources and used without prior purification, except that pyrrole was distilled over KOH before use. *meso*-Triphenylcorrole (**(Ph-Cor)H_3**) was prepared as described previously (Scheme 2) (90).

5-(5-Methyl-2-thienyl)dipyrromethane (S-2)

In a 100 mL round-bottom flask, 1 mL (9.3 mmol) of 5-methyl-2-thiophenecarboxaldehyde (**S-1**) and 4.5 mL (64.9 mmol) of freshly distilled pyrrole were combined and the mixture was degassed with N_2 for 5 min. To this solution, 84 μL (1.1 mmol) of trifluoroacetic acid (TFA) were added via a microsyringe and the mixture was magnetically stirred under an atmosphere of dry N_2 at ambient temperature for 30 min. After this time, thin layer chromatography indicated the formation of dipyrromethane (in a fume hood, fumigation of the dipyrromethane with Br_2 fumes from the headspace of a bromine bottle stains the dipyrromethane bright red). The solution is quenched with 1 mL (7.2 mmol) of Et_3N and diluted with ethyl acetate (50 mL). The organic phase was washed multiple times with water, dried over $MgSO_4$, and reduced to dryness by rotary evaporation. The crude mass was purified by column chromatography (silica–CH_2Cl_2) to provide **S-2** as an off-white solid in 65% yield (1.46 g). The reaction is readily scaled 5-fold. R_f = 0.79 (silica–CH_2Cl_2); ^{1}H NMR (300 MHz, $CDCl_3$): δ = 7.92 (br s, 2H), 6.74-6.68 (m, 4H), 6.25 (m, 2H), 6.13 (s, 2H), 5.65 (s, 1H), 2.53 (s, 3H) ppm; ^{13}C NMR (75 MHz, $CDCl_3$): δ = 143.4, 139.1, 132.2, 125.4, 124.8, 117.5, 108.5, 106.1, 39.4, 15.4 ppm; HR-MS (ESI+, 100% ACN, TOF detection) calculated for $C_{14}H_{15}N_2S$ (M+H): 243.0956, found: 243.0970.

meso-Tris(5-methyl-thien-2-yl)corrole ((S-Cor)H_3)

In a 100 mL round-bottom flask equipped with a stir bar and a gas inlet, 174 μL (1.6 mmol) of 5-methyl-2-thiophenecarboxaldehyde (**S-1**) were dissolved in acetonitrile (60 mL) and the mixture was degassed with N_2 for 5 min. Then, 2.56 g (10.6 mmol) of dipyrromethane **S-2** were added, followed by 120 μL (1.6 mmol) of TFA added via microsyringe, and the solution was stirred at ambient temperature under an N_2 atmosphere. After the consumption of the aldehyde was judged to be complete using gas chromatography (after about 3 h), the reaction was quenched with 450 μL (3.2 mmol) of Et_3N. Next, 1.83 g (8.1 mmol) of 2,3-dichloro-5,6-dicyano-1,4-benzoquinone (DDQ) dissolved in warm toluene (~20 mL) was added to the reaction mixture that was stirred at ambient temperature for 12 h. Removal of the solvent by rotary evaporation and purification of the residue by flash column chromatography (silica–CH_2Cl_2:petroleum ether 2:1) provided the deep green non-polar product **(S-Cor)H_3** in 22% yield (205 mg) in the form of a powder. R_f = 0.85 (silica–CH_2Cl_2:pet ether 2:1); ^{1}H NMR (400 MHz, $CDCl_3$ + 1% TFA): δ = 8.53 (s, 1H), 7.87 (s, 2H), 7.42 (s, 2H), 7.25 (s, 1H) 7.19 (s, 1H), 7.09 (s, 1H), 6.67 (d, 3H) 2.94 (s, 2H), 2.74 (s, 6H), 2.41 (s, 3H), 2.34 (s, 3H); UV-visible (CH_2Cl_2) λ_{max} (log ε): 433 (5.16), 591 (4.18), 641 (4.23) nm; for this spectrum and the spectra in other solvents, see Figure 1; HR-MS (ESI+, 100% ACN, TOF detection) calculated for $C_{34}H_{27}N_4S_3$ (M+H): 587.1398, found: 587.1420.

UV-visible Spectroscopic Methods

All spectra were recorded on a Cary 50 UV-visible spectrophotometer, Agilent Technologies, in 1 cm glass cuvettes in the solvents indicated.

Theoretical Methods

Potential energy surface (PES) scans were systematically performed for each of the three thienyl groups of trithienylcorrole using a Becke, 3-parameter, Lee-Yang-Parr (B3LYP) hybrid functional (91) and a 6-31G(d) basis set, as implemented in Gaussian 09 (92). The geometry of the molecule was optimized following 20° rotational increments around a predefined dihedral angle for each of the three substituents. As the probed group was varied through this rotation, the dihedral angle remained fixed while the rest of the molecule was optimized. The energetics and permanent dipole moment of the molecules throughout each scan were observed to be dependent on the starting conformations of the other two groups of the trisubstituted molecule. Because of this interdependence, the starting orientations of the two freely rotating groups in a scan were modulated based on the position of the sulfur atoms with respect to the macrocycle core. A series of 12 starting conformations were used to accommodate relative differences in substituent orientation. Consequently, a library of 12 local minima was obtained, thereby establishing a reasonable global minimum from the set of PES scans. Tabulation of the resulting dihedral angles, energies, and dipole moments of the minimum from each scan are comprehensively shown in Table S1 (see Supplementary Materials); a subset is shown in Table 1. Subsequently, solvent effects were introduced to the optimized local minima from the PES data set. For simulations involving a solvent environment, the Polarizable Continuum Model (PCM) was employed in Gaussian 09 by using the self-consistent reaction field (SCRF) method (92-94). The local minima obtained

from the PES scans in vacuum were optimized again in a PCM-derived solvent environment and a B3LYP/6-31G(d) method to pinpoint the global minimum in the solvent of interest. The 12 local minima were also used as starting geometries to determine reasonable global minima for the mono-anionic and monocationic molecules. All calculations involving anions included diffuse functions within the basis set (6-31+G(d)) (95).

Although we included diffuse orbitals in our calculations on the anions, we should point out that the simultaneous use of diffuse orbitals and PCM solvent methods remains to be fully substantiated as a viable combination. The problem derives from the fact that a solvent cavity is expected to compact diffuse orbitals significantly. This effect is observed because the energetic advantages of reducing coulombic repulsion are offset by the energetic costs of creating the enlarged solvent cavity necessary to accommodate the diffuse orbitals. At present, theory only partially compensates for these effects. Further work in this area is therefore important.

The excited state properties were calculated using equation-of-motion coupled-cluster with singles and doubles (EOM-CCSD) (96-98) and symmetry-adapted-cluster configuration-interaction (SAC-CI) (99-103) methods. Excited state calculations were all performed using an active space consisting of the eight highest energy filled orbitals and the eight lowest energy virtual orbitals, and by using a Dunning/Huzinaga full double-ζ (D95) basis set (104). Unless otherwise mentioned, the calculated spectroscopic properties were investigated in reference to the Hartree-Fock ground state energies.

Test calculations were initially undertaken to include polarization orbitals in the basis sets of the EOM-CCSD calculations (e.g., a D95(d) basis set instead of D95). In addition to a significant increase in computation time, the results demonstrate that there are negligible differences for the molecules of interest (Figure S1, see Supplementary Materials). We conclude that while including polarization orbitals is very important for the assignment of ground state geometries, the low occupation of these orbitals relegates the additional orbitals of modest importance to the calculation of transition energies and oscillator strengths for the Franck-Condon geometry. We further note that using a D95 basis set is a near optimal choice for EOMCCSD calculations in terms of efficiency and relevant orbital degrees of freedom. Because there is some confusion in the literature on which basis orbitals are included in the D95 basis set, we include Table S3, which formally lists both the orbitals, basis functions and Gaussian primitives that are included for the various basis sets used in this study.

Both the EOM-CCSD and SAC-CI methods yielded reliable results compared to experiment when the PCM solvent environments were included in the simulation (105). The EOM-CCSD methodology has proven to be a reliable method for calculating transition energies and oscillator strengths (96-98, 106, 107). The SAC-CI methods were also used because they provide excited state electron densities and have an excellent history in examining porphyrin systems (99-101, 103, 102). The EOM-CCSD results were plotted in Figure 4 to demonstrate the relative level-ordering of the investigated molecules in various charge states, while SAC-CI analyses in Figures 5, S2, and S3 (see Supplementary Materials) were incorporated to observe the transition energies and transition dipole moments of the first

four excited states. We found that the combined use of EOM-CCSD and SAC-CI methods provided a good perspective on the excited state properties of these molecules.

RESULTS AND DISCUSSION

Synthesis

The synthesis of the triarylcorroles investigated was accomplished using an established methodology (Scheme 2) (90). A dipyrromethane **2**, prepared from pyrrole and an arylaldehyde, **1**, is converted to a triaryl-tetrapyrrane **3** that is, without prior isolation, oxidatively ring-closed to the corresponding corrole (90). The *meso*-tris(5-methyl-thien-2-yl)corrole (**(S-Cor)H$_3$**) thus prepared from 5-methyl-thienyl-2-aldehyde (**S-1**) and pyrrole showed all the expected spectroscopic and analytical properties. The corrole and the intermediate 5-(5-methylthien-2-yl)dipyrromethane (**S-2**) are both similar to the parent non-methylated thienyl derivatives firstly prepared by Churchill (82, 80). We chose the 5-methyl substituted derivative because we have shown that the 5-methyl group lead to a further red-shift of the optical spectra in *meso*thienyl-substituted porphyrins (59). Also, the substitution of the thienyl α-position shuts down possible degradation processes at this reactive position.

Empirical UV-visible Spectra of the Corroles

The conventional approach of describing the steady-state absorption spectra of corroles is to assign the transitions in the UV-visible domain as those observed for the parent porphyrin complexes (28). Thus, absorption bands in the 400 nm region are assigned as B-bands (i.e., Soret-like transitions), and all those of lower energy (500-700 nm) are considered as Q bands. Accordingly, transitions to the S_1, S_2, S_3, and S_4 energy levels of triarylcorroles will be considered analogous to the transitions of porphine to be the Q_x, Q_y, B_x, and B_y bands, respectively. We follow this labeling scheme hereafter to describe the empirical designation of the electronic transitions.

The UV-visible spectra of **(Ph-Cor)H$_3$** and **(S-Cor)H$_3$** in the non-polar solvent dichloromethane (CH_2Cl_2, DCM) and in the polar solvent acetonitrile (CH_3CN, ACN) are presented in Figure 1. Both porphyrins and corroles are dominated by $\pi^* \leftarrow \pi$ transitions, contain an intense Soret band at ~400 nm, and exhibit a set of Q transitions at energies lower than 500 nm. As was described before, electronic transitions of corroles tend to be of lower energy than of the related porphyrin macrocycles (28). Furthermore, a relative decrease in the extinction coefficient of the Soret bands with respect to the Q bands are commonly observed in corrole spectra due to the decreased symmetry of the macrocycle.

The absorption spectra of the *meso*-phenyl derivative, **(Ph-Cor)H$_3$**, and *meso*-thienyl derivative, **(S-Cor)H$_3$**, in DCM contain similar transitions and relative ratios between the Soret and Q bands, but there are some notable differences. The Soret band of **(S-Cor)H$_3$** is red-shifted by 17 nm compared to that of **(Ph-Cor)H$_3$** (433 and 416 nm, respectively), and it is significantly broader. As described before, the Q band region of **(Ph-Cor)H$_3$** consists of three primary bands, at 574, 617, and 651 nm (28). In comparison, the Q bands in the **(S-Cor)H$_3$** spectrum at 592, 647, and 682 nm, with a possible feature appearing at 754 nm, are 18-31 nm red-shifted and far less discrete. There is also a noticeable increase in oscillator

strength of these bands relative to the Soret band. These differences are consistent with previous findings that corrole absorption spectra are characteristically subject to *meso*-substituent-dependent shifts (28).

Corrole absorption spectra (and also a number of other physical and chemical properties) are also prone to significant solvatochromic effects (108, 109, 26-28) that were described and rationalized before. Thus, for both corroles a significant red shift of the Q band region is observed in the strongly polar solvent ACN relative to the non-polar solvent DCM. **(Ph-Cor)H_3** demonstrates an altered Q band structure with two distinct absorption peaks at 580 and 638 nm, in which the 638 nm band has a higher relative oscillator strength than any other feature in the non-polar solvent. The Q band region of **(S-Cor)H_3** also exhibits an intense two band structure (591 and 641 nm). This difference in the absorption spectra is interesting and we will present below a theoretical investigation to elucidate the role the thienyl groups play in the solvatochromism of the thienylcorroles. The position of the Soret bands of **(Ph-Cor)H_3** and **(SCor)H_3**, however, are immune to any solvatochromic effect in these solvents.

The acid-base equilibria of corroles were also well described before (15, 23, 26, 110). Scheme 3 describes this acid-base equilibrium, and establishes the nomenclature for the mono-anionic and mono-cationic forms of the triarylcorroles. Corroles are intrinsically much more acidic than porphyrins (23). Consequently, even mild bases were shown to be capable of generating the anionic form of triarylcorroles (15, 23, 26, 110). This high acidity can be attributed to the relief of steric hindrance upon the loss of a hydrogen within the inner core of the corrole. This acidity is solvent dependent and is sensitive to the nature of the *meso*-substituents (15, 23, 26, 110). Addition of the non-nucleophilic strong base, 1,8-diazabicyclo[5.4.0]undec-7-ene (DBU), to **(Ph-Cor)H_3** and **(S-Cor)H_3** in DCM invariably leads to the formation of the anionic forms **[(Ph-Cor)H_2]$^-$** and **[(S-Cor)H_2]$^-$**, as indicated by the appearance of an intense band at 639 and 652 nm, respectively. Electronic differences between the corroles carrying the two different types of *meso*-substituents are apparent in the Soret band of **[(Ph-Cor)H_2]$^-$**, which is split into two distinct peaks.

On the other hand, addition of the strong organic acid, TFA, mono-protonates the triarylcorroles, creating **[(Ph-Cor)H_4]$^+$** and **[(S-Cor)H_4]$^+$** (10, 23, 111). The cationic configuration of the molecules produce an absorption band in the Q band region that has a larger bathochromic shift, with an intense peak for the phenyl- and thienyl-containing molecules at 666 and 679 nm, respectively. Again, significant differences for the two different corroles are visible. For instance, **[(S-Cor)H_4]$^+$** exhibits a dramatically decreased Soret band to Q band ratio, whereas the **[(Ph-Cor)H_4]$^+$** Soret band again splits into two peaks.

Below we examine the important conformational influences with regard to the formation of both the mono-anionic and mono-cationic species, as well as the relevance of acid-base chemistry in the solvatochromism of the corroles. We also investigate the apparent differences between the formations of these ions in **(Ph-Cor)H_3** and **(S-Cor)H_3** to determine the influence of the thienyl substituents on the formation of the anionic/cationic forms.

Structural and Conformational Investigations of Triarylcorroles

The neutral forms of the triarylcorroles are characterized by a trivalent cavity that is in dynamic equilibrium between the two distinct tautomers, 1 and 2 (Scheme 3) (25, 27, 112). The tautomeric equilibrium is solvent and temperature dependent (25, 27). Ding *et al.* investigated the crystal structure of **(Ph-Cor)H_3** and found that tautomer 2 is the preferred configuration (112). Our own ground state geometric analyses also suggested that tautomer 2 is universally more stable, both *in vacuo* and within all solvent environments, irrespective of the nature of the *meso*-aryl groups (here, phenyl or thienyl). Hence, the hydrogen configuration corresponding to tautomer 2 will be used in all subsequent discussions of the neutral triarylcorroles.

Similarly, while the two hydrogens of the anionic core are capable of arranging in multiple configurations, our calculated group state energies predicted that the hydrogen atoms are oriented diagonal from each other in the macrocycle core. This conformation is also the preferred arrangement in the analogous free-base porphyrin structures (113). The mono-cationic species, of course, is capable of only one configuration with respect to the core hydrogen atoms.

Because each of the three *meso*-aryl substituents on the corrole macrocycle are able to rotate around the *meso*-*ipso*-bond, there are a number of local energy minima available to the molecule. This effect is particularly critical for **(S-Cor)H_3**, where the relative positions of the three non-axial symmetric aryl groups influence the planarity of the flexible macrocycle core and the total dipole moment of the molecule, and thus, the spectroscopic properties of the corrole. Thus, potential energy surface (PES) scans were performed to determine the lowest energy ground state geometry of both **(Ph-Cor)H_3** and **(S-Cor)H_3**.

The PES scans were first carried out *in vacuo*, with 12 varying starting positions of the substituents. Figure 2a illustrates the three $C^{ß}$(thienyl)-$C^{α}$(thienyl)-C^{meso}(corrole)-$C^{α}$(corrole) dihedral angles ϕ_1 through δ_3 that were monitored throughout the three possible PES scans. Because of the asymmetry of the corrole macrocycle, the rotational itineraries for all three thienyl groups vary from each other (Figure 2b). These curves are also highly reliant on the relative position of the other two groups of the molecule, which have an impact on the macrocycle conformation. Consequently, the PES scans presented in Figure 2b are only one combinatorial example of the energetics of this molecule.

Table S1 (see Supplementary Materials) shows the results of a series of PES scans that were undertaken, which systematically investigated the possible combinations of starting orientations of the thienyl groups. The data shows the lowest energy conformation of each PES scan, or a selection of 12 local energy minima (molecules **1**-**12** in Table S1). *In vacuo*, the **(SCor)H_3** molecule with the lowest energy conformation has a calculated heat of formation (HOF) of ~963 kJ/mol. Table 1 lists the global minima found.

Subsequently, the 12 local energy minima conformations were minimized in solvent (DCM and ACN) by using PCM solvent methods. Figure 2a tabulates the thienyl group conformations (expressed as the dihedral angles δ_1 through δ_3) corresponding to the global minima in the solvents indicated. It also lists the dipole moment and HOF for each molecule.

Note that while the addition of non-polar solvent did not have a significant impact on the lowest energy geometry, the inclusion of ACN showed that the lowest energy conformation molecule had, as expected, the highest dipole moment.

The 12 local energy minima derived from the *in vacuo* optimizations were also used as starting conformations to determine the lowest energy conformations of the mono-anionic and mono-cationic forms of the triarylcorroles. Table 1 lists the ground state energies of these molecules in solvent used for the excited state calculations.

Overall, two major findings can be derived. Firstly, the ground state energy of the molecule is largely dependent on the relative orientation of each of the three thienyl groups, and thus, is strongly coupled to the permanent dipole moment of the structure. Thus, the dipole moment and ground state energy have a strong relationship with the solvent environment, particularly in polar solvents. Secondly, the conformations selected in Table 1 delineate reasonable global minima in varying solvents for the subsequent theoretical investigations.

The relative acidity and basicity of the triarylcorroles depends on the electronic interaction of the *meso*-substituents with the macrocycle core. However, the difference in electron withdrawing effects between the thienyl and phenyl substituents is small and likely inconsequential to relative acidities (see Supplementary Materials, Table S2). The acidity of the core is tied more closely to the constrained nature of the corrole, the planarity of the macrocycle, and the co-planarity of the substituents with the macrocycle. Figure 3 presents a linear display of the deviation of the 23 atoms that comprise the macrocycle framework from a mean plane defined by the three C^{meso} atoms. The conformation of the pyrrole rings is strongly dependent on the rotational freedom of the tri-substituted corroles, and it is the magnitude of the deviation that is of interest here, not necessarily the directionality of the deviation.

The modes of deviation from planarity of the computed neutral **(Ph-Cor)H_3** and **(S-Cor)H_3** are similar in magnitude and are characteristic of what is also commonly observed in the crystal structures of triarylcorroles (10, 80, 81). The contracted macrocycle core and the presence of three hydrogen atoms introduces a steric clash in the center of the macrocycle. To relieve this, the macrocycle plane takes up a saddling distortion.

Removal of a hydrogen results in a large decrease of the steric clash and results in the formation of strong intramolecular H-bonds. This planarization and overall energy release is at the origin of the high acidity of corroles (23). Deprotonation also planarizes the macrocycles in **[(Ph-Cor)H_2]$^-$** and **[(S-Cor)H_2]$^-$** and significantly lowers the energy of the molecules (cf. Table 1). Notably, **[(Ph-Cor)H_2]$^-$** is significantly more planar than **[(S-Cor)H_2]$^-$**. Considering the smaller steric interaction of the thienyl groups with the parent macrocycle, this finding is counter-intuitive.

The conformation of the mono-protonated forms of the corroles also shows a strong dependence on the nature of the *meso*-substituents. The protonated form of the *meso*-thienyl-substituted corrole, **[(S-Cor)H_4]$^+$**, is significantly more non-planar than the phenyl-containing corrole, yet its energy increase relative to the non-protonated form is 26/28 kJ/mol less than for the phenyl-derivative (in vacuum/DCM). This difference between the

phenyl- and thienyl-substituted mono-protonated corroles is also reflected in the UV-visible absorption spectra of **[(S-Cor)H$_4$]$^+$** and **[(Ph-Cor)H$_4$]$^+$** (Figure 1), particularly in terms of the relative oscillator strengths of the Soret and Q bands and the bathochromic shift of the Q-bands. Table 2 lists the dihedral angles of the mono-cationic forms of **(Ph-Cor)H$_3$** and **(S-Cor)H$_3$**. The thienyl groups are more co-planar with the corrole chromophore than the phenyl groups are, thus allowing a strong coupling of the thienyl π-system with that of the corrole. In general, corroles exhibit an increase in the extinction coefficients of the Q bands due to the reduction of alternancy symmetry (114). The out-of-plane conformation of **[(S-Cor)H$_4$]$^+$** further reduces the chromophore symmetry. This, together with the added charge through protonation and the extended π-system involving the thienyl groups (see also below) rationalize the unique spectral features of this species.

Again, we like to highlight the counter-intuitive finding that the sterically less encumbered thienyl groups lead to a more non-planar chromophore. However, this finding is mirrored by precedence. Protonated thienyl-substituted porphyrins were also observed to be significantly more deplanarized than the corresponding protonated phenyl-substituted derivative (59). We attribute this to an effect where the larger (but presumably still small) loss of π-conjugation induced by the non-planar conformation is balanced by the increased π-conjugation with the thienyl groups this conformation enables. On the other hand, the larger phenyl groups will not, even at the highly non-planar conformations, be allowing an equivalent co-planarity of the π-systems, thus not providing to such an extent a stabilizing π-overlap. The fact that this effect is most prominent in the protonated cases might be due to the additional driving forces of the accumulated charges in the center of the macrocycles, the dissipation of which is also assisted by the π-conjugation effects evoked. The charge density maps of the Soret transitions of **[(S-Cor)H$_4$]$^+$** (see Supplementary Materials, Figure S3) show this conjugative stabilization. The conjugation effects of the thienyl groups with porphyrins was also cited by Bhyrappa *et al*. to rationalize the optical properties of *meso*-thienyl-substituted porphyrins (63).

The Excited State Properties of Triarylcorroles

To describe the nature of the electronic transitions of **(Ph-Cor)H$_3$** and **(S-Cor)H$_3$**, a combination of SAC-CI and EOM-CCSD excited state calculations were used to determine relative level ordering, transition energies, and transition dipole moments of the molecules.

Figure 4 shows the predicted level ordering of the first 4 excited states of **(Ph-Cor)H$_3$** and **(S-Cor)H$_3$** in neutral, mono-anionic, and mono-cationic forms, as predicted by using EOMCCSD coupled-cluster methods and PCM solvent (DCM and ACN) environments. It is evident that all of the computed energy levels of the thienyl derivative, **(S-Cor)H$_3$**, are lower in energy than the corresponding levels of the phenyl derivative **(Ph-Cor)H$_3$**. The energy drop is concomitant with a reduction of the HOMO–LUMO gap. This is also supported experimentally by their UV-visible spectra (see Figure 1). Furthermore, the computed oscillator strengths of the Q bands of **(S-Cor)H$_3$** are larger, the S_3 and S_4 transitions are further separated in energy (i.e., the Soret band is broader), and the general Soret-band to Q band ratio is also consistently smaller for the neutral molecules. Again, this is supported by the experimental UV-visible spectra.

What is striking, however, is the seemingly small solvatochromatic effect that was computed for both **(Ph-Cor)H_3** and **(S-Cor)H_3**. The energy level ordering and oscillator strengths of the transitions are essentially identical between **(Ph-Cor)H_3** in DCM and ACN and between **(S-Cor)H_3** in the same solvent set. Figure 5 includes a SAC-CI analysis of the first 4 excited states of **(Ph-Cor)H_3** and **(S-Cor)H_3**. Here, it also becomes apparent that the thienyl-containing molecules have lower transition energies than the phenyl analogue, however, the transition energies are similar when comparing each molecule in non-polar and polar solvents. These results are consistent with a recent study using Time-Dependent Density Functional Theory (TD-DFT), which also predicted that there is little solvatochromism for the $\pi^* \leftarrow \pi$ transitions for triarylcorroles (17). Acetonitrile enhances the transition dipole moments of the molecules, with a much greater effect observed for **(S-Cor)H_3** than the triphenyl derivative. Furthermore, both molecules are energetically stabilized in ACN (Table 1) (for conformers with high dipole moments). However, predictions suggest little solvent effect on the photochemistry of the neutral molecules.

Although the excited state calculations indicate little solvatochromism, the experimental data in Figure 1 paint a different picture, particularly for **(Ph-Cor)H_3**. The absorption spectrum of **(Ph-Cor)H_3** in ACN contains a strongly absorbing peak at 639 nm, which is not observed in DCM. We suggest that the formation of the anionic species **[(Ph-Cor)H_2]$^-$** is the source of the observed solvatochromic shift (26). **[(Ph-Cor)H_2]$^-$** is more planar in ACN than **[(S-Cor)H_2]$^-$**, thus making the phenyl-containing corrole more acidic (i.e., more likely to deprotonate).

Figure S2 (see Supplementary Materials) presents a collection of SAC-CI excited state analyses, in which the transition energies, transition dipole moments, and relative electrostatic characteristics are tabulated for the mono-anionic species in both DCM and ACN. In addition to the HOF analysis in the discussion above (Table 1), the transition energies of **[(Ph-Cor)H_2]$^-$** in ACN are generally lower than the transition energies observed for **(Ph-Cor)H_3** in the same solvent. On the other hand, the opposite is true of **[(S-Cor)H_2]$^-$** and **(S-Cor)H_3** in ACN, where the transition energies are roughly equivalent or lower for the neutral molecule. This provides further evidence that the solvent and electronic nature of **(Ph-Cor)H_3** make this corrole derivative more acidic than **(S-Cor)H_3** in the same solvent, and that the apparent solvatochromism results from apparent deprotonation events (26).

The theoretical mono-cationic data is consistent with empirical observations (see Figures 1 and 4). While the Q_x band of **[(Ph-Cor)H_4]$^+$** is characterized by a relatively high oscillator strength (f = 0.234), **[(S-Cor)H_4]$^+$** exhibits a dramatically amplified oscillator strength (f = 0.525). Additionally, the Soret bands of **[(S-Cor)H_4]$^+$** stray from all other experimental observations for the triarylcorroles, in which the S_3 transition is much lower in oscillator strength (f = 1.074) and contains significantly less ionic character. These optical effects have much to do with the loss of planarity and the accommodation of π-overlap, thereby enhancing the electronic interaction between the thienyl groups and macrocycle. The loss of ionic character is linked to the degeneration of the pseudoparity of the molecular orbitals along the macrocycle, which has already significantly diminished when going from the porphyrin parent compounds to the corrole structure (114). This loss of alternancy symmetry is intensified by the molecular structure of the mono-cation and has severe optical

consequences. The S_3 transition, specifically, is characterized by large doubly excited configurational character (Figures 6 and S2, see Supplementary Materials), which suggests that this state is more covalent in nature and has less charge separation of the molecular orbitals. Moreover, the SAC-CI analysis in Figure S3 (see Supplementary Materials) indicates that **[(S-Cor)H$_4$]$^+$** has diminished transition dipole moments relative to all other molecules in this investigation, which is further evidence of decreased ionic character of the molecule.

In order to determine the source of the unique spectroscopic properties that are observed and predicted for **(S-Cor)H$_3$**, the configurational character of the triarylcorroles must be considered. Ziegler *et al*. have recently studied free-base triarylcorroles by using TD-DFT and magnetic circular dichroism (MCD) to examine the optical properties and solvatochromic effects (17). This study has found a rare relationship within the π and π* molecular orbitals (MOs) of the free-base corrole core, in which there is a larger energy difference between LUMO and LUMO+1 π* MOs (ΔLUMO) compared to HOMO and HOMO-1 π MOs (ΔHOMO). This scheme is opposite that of Gouterman's four orbital model of porphyrins (115). Figure 6 depicts the configurational properties of the first four excited states of **(Ph-Cor)H$_3$** and **(S-Cor)H$_3$**, as predicted by SAC-CI MO theory. The ΔHOMO < ΔLUMO relationship is confirmed in using this model, however, analysis of the configurational character of the two molecules reveal a higher complexity over simple porphyrins.

The four orbital model works generally well with these molecules, however, there is significant mixing between the energy levels and a large contribution from double excitations. The configurational description of the Q band region for **(Ph-Cor)H$_3$** and **(S-Cor)H$_3$** are surprisingly similar. The character of the Soret bands of **(S-Cor)H$_3$** differ more significantly compared to **(Ph-Cor)H$_3$**. The thienyl-substituted molecule has a large degree of mixing and doubly excited character in the Soret region, and an even larger deviation from the four orbital model. The MO configurations of **(S-Cor)H$_3$**, as well as the enhanced π-overlap of the substituents, indicate a complex electronic structure that is subject to unique chromatic shifts and sensitivities to acidic and basic solvent environments.

CONCLUSIONS

The photophysical properties of free-base *meso*-trithienylcorroles were investigated in direct comparison to *meso*-triphenylcorroles, which have a broad history of investigations throughout the literature. The origin of the unique electronic characteristics of the trithienylcorrole were described using a combinational approach of spectroscopic and theoretical methodologies. This work complements a number of other reports that elucidated other aspects of the electronic structure of *meso*-arylcorroles and the much increased electronic cross-talk between the *meso*substituents and the chromophore when compared to *meso*-arylporphyrins. This study is the first to implement EOM-CCSD and SAC-CI excited state calculations. The ground state and excited state calculations generally support experimental findings, wherein the trithienylcorroles posses red-shifted optical spectra compared to the corresponding triphenylcorroles, irrespective of whether they are in the neutral, deprotonated, or protonated states. Theoretical approaches by using PES scans were

incorporated into a series of ground state minimizations, in an attempt to delineate reasonable global energy minima for molecules that are highly flexible, rotationally variable, and sensitive to solvent environments. Solvatochromic behavior is rationalized based on conformational and dipole effects, although it was found that the formation of the mono-anionic molecules are energetically favorable and likely explain the dramatic shifts in the optical spectra. At the same charge state, it was found that **(S-Cor)H_3** adopts a more non-planar conformation than **(Ph-Cor)H_3**, thus allowing a larger degree of co-planarity and electronic interaction of the thienyl groups with the corrole chromophore. The key differences in the configurational character of the two molecules of interest were also explained. The experimental differences can be rationalized once this data is coupled with the relative MO energies and the structural characteristics described above. The complex nature of the configurational character of the Soret bands and the large degree of mixing also provide insight into the unique optical effects observed of **(S-Cor)H_3** in this investigation.

In conclusion, thienylcorroles are interesting corrole derivatives in that the thienyl groups have a profound effect on the electronic properties of the chromophore. The reactivity of the thiophene moiety presumably allows the thienylcorroles, like its porphyrin congeners, to be incorporated into conducting polymer networks but that might benefit from the tight coupling of the *meso*-substituents with the corrole chromophore. We look forward to the ongoing developments in this and related fields.

Supplementary Material

Refer to Web version on PubMed Central for supplementary material.

Acknowledgments

This work was supported by the US National Science Foundation (NSF) through grants CHE-0517782 and CHE-1058846 (to CB), the National Institutes of Health through GM-34548 (to RRB), a Pfizer Undergraduate Summer Research Fellowship (to AR), and the Harold S. Schwenk Sr. Distinguished Chair in Chemistry (to RRB). The departmental 400 MHz NMR was supported by the NSF (CHE-1048717).

REFERENCES

1. Battersby AR. Tetrapyrroles: the pigments of life. Nat. Prod. Rep. 2000; 17:507–526. [PubMed: 11152419]
2. Toganoh, M.; Furuta, H. Synthesis and metal coordination of N-confused and N-fused porphyrinoids.. In: Kadish, KM.; Smith, KM.; Guilard, R., editors. In Handbook of Porphyrin Science. Vol. 2. World Scientific; Singapore: 2010. p. 295-367.
3. Lash, TD. Carbaporphyrins and related systems. Synthesis, characterization, reactivity and insights into porphyrinoid aromaticity.. In: Kadish, KM.; Smith, KM.; Guilard, R., editors. In Handbook of Porphyrin Science. Vol. 16. World Scientific; Singapore: 2010. p. 1-330.
4. Kadish, KM.; Smith, KM.; Guilard, R. The Porphyrin Handbook, Vol. 2 - Heteroporphyrins, Expanded Porphyrins and Related Macrocycles. Vol. 2. Academic Press; San Diego: 2000.
5. Fox S, Boyle RW. Synthetic routes to porphyrins bearing fused rings. Tetrahedron. 2006; 62:10039–10054.
6. Gupta I, Ravikanth M. Recent developments in heteroporphyrins and their analogues. Coord. Chem. Rev. 2006; 250:468–518.
7. Stepien M, Latos-Grazynski L. Benziporphyrins: Exploring arene chemistry in a macrocyclic environment. Acc. Chem. Res. 2005; 38:88–98. [PubMed: 15709728]

8. Stepien M, Latos-Grazynski L. Aromaticity and tautomerism in porphyrins and porphyrinoids. Top. Heterocycl. Chem. 2009; 19:83–153.
9. Pawlicki, M.; Latos-Grazynski, L. Carbaporphyrinoids — synthesis and coordination properties.. In: Kadish, KM.; Smith, KM.; Guilard, R., editors. In Handbook of Porphyrin Science. Vol. 2. World Scientific; Singapore: 2010. p. 103-192.
10. Aviv-Harel I, Gross Z. Aura of corroles. Chem.–Eur. J. 2009; 15:8382–8394. [PubMed: 19630016]
11. Gross Z, Galili N, Saltsman I. The first directed synthesis of corroles from pyrrole. Angew. Chem. Int. Ed. Engl. 1999; 38:1427–1429.
12. Gross Z, Galili N, Simkhovich L, Saltsman I, Botoshansky M, Bläser D, Boese R, Goldberg I. Solvent-free condensation of pyrrole and pentafluorobenzaldehyde: A novel synthetic pathway to corrole and oligopyrromethenes. Org. Lett. 1999; 1:599–602.
13. Gryko DT. Recent advances in the synthesis of corroles and core-modified corroles. Eur. J. Org. Chem. 2002:1735–1743.
14. Gryko DT, Fox JP, Goldberg DP. Recent advances in the chemistry of corroles and core-modified corroles. J. Porphyrins Phthalocyanines. 2004; 8:1091–1105.
15. Nardis S, Monti D, Paolesse R. Novel aspects of corrole chemistry. Mini-Rev. Org. Chem. 2005; 2:355–374.
16. Gryko DT. Adventures in the synthesis of meso-substituted corroles. J. Porphyrins Phthalocyanines. 2008; 12:906–917.
17. Ziegler CJ, Sabin J, Geier III GR, Nemykin VN. The first TDDFT and MCD studies of free base triarylcorroles: A closer look into solvent-dependent UV-visible absorption. Chem. Commun. 2012; 48:4743–4745.
18. Alemayehu A, Conradie J, Ghosh A. A first TDDFT study of metallocorrole electronic spectra: Copper meso-triarylcorroles exhibit hyper spectra. Eur. J. Inorg. Chem. 2011; 2011:1857–1864.
19. Ghosh A, Steene E. High-valent transition metal centers and noninnocent ligands in metalloporphyrins and related molecules: A broad overview based on quantum chemical calculations. J. Biol. Inorg. Chem. 2001; 6:740–751.
20. Rovira C, Kunc K, Hutter J, Parrinello M. Structural and electronic properties of Co-corrole, Co-corrin, and Co-porphyrin. Inorg. Chem. 2001; 40:11–17. [PubMed: 11195367]
21. Steene E, Wondimagegn T, Ghosh A. Resonance Raman spectroscopy and density functional theoretical calculations of manganese corroles. A parallelism between high-valent metallocorroles and metalloporphyrins, relevant to horseradish peroxidase and chloroperoxidase compound I and II intermediates. J. Inorg. Biochem. 2002; 88:113–118. [PubMed: 11750033]
22. Wasbotten IH, Wondimagegn T, Ghosh A. Electronic absorption, resonance Raman, and electrochemnical studies of planar and saddled copper(III) meso-triarylcorroles. Highly substituent-sensitive Soret bands as a distinctive feature of high-valent transition metal corroles. J. Am. Chem. Soc. 2002; 124:8104–8116. [PubMed: 12095356]
23. Mahammed A, Weaver JJ, Gray HB, Abdelas M, Gross Z. How acidic are corroles and why? Tetrahedron Lett. 2003; 44:2077–2079.
24. Ghosh A, Wondimagegn T, Parusel BJ. Electronic structure of gallium, copper, and nickel complexes of corrole. High-valent transition metal centers versus noninnocent ligands. J. Am. Chem. Soc. 2000; 122:5100–5104.
25. Ivanova YB, Savva VA, Mamardashvili NZ, Starukhin AS, Ngo TH, Dehaen W, Maes W, Kruk MM. Corrole NH tautomers: Spectral features and individual protonation. J. Phys. Chem. A. 2012; 116:10683–10694. [PubMed: 22985133]
26. Kruk M, Ngo TH, Savva V, Starukhin A, Dehaen W, Maes W. Solvent-dependent deprotonation of meso-pyrimidinylcorroles: Absorption and fluorescence studies. J. Phys. Chem. A. 2012; 116:10704–10711. [PubMed: 22985221]
27. Kruk M, Ngo TH, Verstappen P, Starukhin A, Hofkens J, Dehaen W, Maes W. Unraveling the fluorescence features of individual corrole NH tautomers. J. Phys. Chem. A. 2012; 116:10695–10703. [PubMed: 22985194]
28. Ding T, Alemán EA, Modarelli DA, Ziegler CJ. Photophysical properties of a series of free-base corroles. J. Phys. Chem. A. 2005; 109:7411–7417. [PubMed: 16834109]

29. Wagnert L, Berg A, Stavitski E, Berthold T, Kothe G, Goldberg I, Mahammed A, Simkhovich L, Gross Z, Levanon H. Exploring the photoexcited triplet states of aluminum and tin corroles by time-resolved Q-band EPR. Appl. Magn. Reson. 2006; 30:591–604.
30. Rozenshtein V, Wagnert L, Berg A, Stavitski E, Berthold T, Kothe G, Saltsman I, Gross Z, Levanon H. Probing the photoexcited states of rhodium corroles by time-resolved Q-band EPR. Observation of strong spin-orbit coupling effects. J. Phys. Chem. A. 2008; 112:5338–5343. [PubMed: 18507363]
31. Wagnert L, Berg A, Saltsman I, Gross Z, Rozenshtein V. Time-resolved electron paramagnetic resonance study of rhodium(III) corrole excited states. J. Phys. Chem. A. 2010; 114:2059–2072. [PubMed: 20070101]
32. Wagnert L, Rubin R, Berg A, Mahammed A, Gross Z, Levanon H. Photoexcited triplet state properties of brominated and nonbrominated Ga(III)-corroles as studied by time-resolved electron paramagnetic resonance. J. Phys. Chem. B. 2010; 114:14303–14308. [PubMed: 20112985]
33. Tanabe M, Matsuoka H, Ohba Y, Yamauchi S, Sugisaki K, Toyota K, Sato K, Takui T, Goldberg I, Saltsman I, Gross Z. Time-resolved electron paramagnetic resonance and phosphorescence studies of the lowest excited triplet states of Rh(III) corrole complexes. J. Phys. Chem. A. 2012; 116:9662–9673. [PubMed: 22946766]
34. Yang Y, Jones D, von HT, Linke M, Wagnert L, Berg A, Levanon H, Zacarias A, Mahammed A, Gross Z, Heyne K. Assignment of aluminum corroles absorption bands to electronic transitions by femtosecond polarization resolved VIS-pump IR-probe spectroscopy. J. Phys. Chem. A. 2012; 116:1023–1029. [PubMed: 22201283]
35. Brückner C. The silver complexes of porphyrins, corroles and carbaporphyrins: Silver in the oxidation states +II and +III. J. Chem. Educ. 2004; 81:1665–1670.
36. Gross Z, Gray HB. How do corroles stabilize high valent metals? Comments Inorg. Chem. 2006; 27:61–72.
37. McGown, AJ.; Badiei, YM.; Leeladee, P.; Prokop, KA.; DeBeer, S.; Goldberg, DP. Synthesis and reactivity of high-valent transition metal corroles and corrolazines.. In: Kadish, KM.; Smith, KM.; Guilard, R., editors. In Handbook of Porphyrin Science. Vol. 14. World Scientific; Singapore: 2011. p. 525-599.
38. Gross Z, Golubkov G, Simkhovich L. Epoxidation catalysis by a manganese corrole and isolation of an oxomanganese(V) corrole. Angew. Chem. Int. Ed. 2000; 39:4045–4047. [PubMed: 11093199]
39. Simkhovich L, Mahammed A, Goldberg I, Gross Z. Synthesis and characterization of germanium, tin, phosphorus, iron, and rhodium complexes of tris(pentafluorophenyl)corrole, and the utilization of the iron and rhodium corroles as cyclopropanation catalysts. Chem.–Eur. J. 2001; 7:1041–1055. [PubMed: 11303864]
40. Aviv I, Gross Z. Iron corroles and porphyrins as very efficient and highly selective catalysts for the reactions of α-diazo esters with amines. Synlett. 2006:951–953.
41. Mahammed A, Gross Z. Iron and manganese corroles are potent catalysts for the decomposition of peroxynitrite. Angew. Chem., Int. Ed. 2006; 45:6544–6547.
42. Eckshtain M, Zilbermann I, Mahammed A, Saltsman I, Okun Z, Maimon E, Cohen H, Meyerstein D, Gross Z. Superoxide dismutase activity of corrole metal complexes. Dalton Trans. 2009:7879–7882. [PubMed: 19771348]
43. Kumar A, Goldberg I, Botoshansky M, Buchman Y, Gross Z. Oxygen atom transfer reactions from isolated (oxo)manganese(V) corroles to sulfides. J. Am. Chem. Soc. 2010; 132:15233–15245. [PubMed: 20932015]
44. Schechter A, Stanevsky M, Mahammed A, Gross Z. Four-electron oxygen reduction by brominated cobalt corrole. Inorg. Chem. 2012; 51:22–24. [PubMed: 22221278]
45. Aviv I, Gross Z. Corrole-based applications. Chem. Commun. 2007:1987–1999.
46. Aviv-Harel I, Gross Z. Coordination chemistry of corroles with focus on main group elements. Coord. Chem. Rev. 2011; 255:717–736.
47. Walker D, Chappel S, Mahammed A, Brunschwig BS, Winkler JR, Gray HB, Zaban A, Gross Z. Corrole-sensitized TiO_2 solar cells. J. Porphyrins Phthalocyanines. 2006; 10:1259–1262.

48. Kim K, Kim I, Maiti N, Kwon SJ, Bucella D, Egorova OA, Lee YS, Kwak J, Churchill DG. A study of nerve agent model organophosphonate binding with manganese-A_2B-corrole and -A_2B_2-porphyrin systems. Polyhedron. 2009; 28:2418–2430.
49. Aviezer D, Cotton S, David M, Segev A, Khaselev N, Galili N, Gross Z, Yayon A. Porphyrin analogues as novel antagonists of fibroblast growth factor and vascular endothelial growth factor receptor binding that inhibit endothelial cell proliferation, tumor progression, and metastasis. Cancer Res. 2000; 60:2973–2980. [PubMed: 10850445]
50. Wang Y, Akhigbe A, Ding Y, Brückner C, Lei Y. meso-Tritolylcorrolefunctionalized single-walled carbon nanotube donor-accepter nanocomposites for NO_2 gas detection. Electroanalysis. 2012; 24:1348–1355.
51. Haber A, Aviram M, Gross Z. Protecting the beneficial functionality of lipoproteins by 1-Fe, a corrole-based catalytic antioxidant. Chem. Sci. 2011; 2:295–302.
52. Hwang JY, Wachsmann-Hogiu S, Ramanujan VK, Ljubimova J, Gross Z, Gray HB, Medina-Kauwe LK, Farkas DL. A multimode optical imaging system for preclinical applications in vivo: Technology development, multiscale imaging, and chemotherapy assessment. Mol. Imaging Biol. 2012; 14:431–442. [PubMed: 21874388]
53. Lim P, Mahammed A, Okun Z, Saltsman I, Gross Z, Gray HB, Termini J. Differential cytostatic and cytotoxic action of metallocorroles against human cancer cells: Potential platforms for anticancer drug development. Chem. Res. Toxicol. 2012; 25:400–409. [PubMed: 22185566]
54. Haber A, Angel I, Mahammed A, Gross Z. Combating diabetes complications by 1-Fe, a corrole-based catalytic antioxidant. J. Diabetes Complications. 2013; 27:316–321. [PubMed: 23602197]
55. Ojadi ECA, Linschitz H, Gouterman M, Walter RI, Lindsey JS, Wagner RW, Droupadi PR, Wang W. Sequential protonation of meso-[p-(dimethylamino)phenyl]porphyrins: Charge-transfer excited states producing hyperporphyrins. J. Phys. Chem. 1993; 97:13192–13197.
56. Vitasovic M, Gouterman M, Linschitz H. Calculations on the origin of hyperporphyrin spectra in sequentially protonated meso-(dimethylaminophenyl) porphyrins. J. Porphyrins Phthalocyanines. 2001; 5:191–197.
57. Thomas DW, Martell AE. Absorption spectra of para-substituted tetraphenylporphines. J. Am. Chem. Soc. 1956; 78:1338–1343.
58. Senge, MO. Database of tetrapyrrole crystal structure determinations.. In: Kadish, KM.; Smith, KM.; Guilard, R., editors. In Porphyrin Handbook. Vol. 10. Academic Press; San Diego: 2000. p. 1-218.
59. Brückner C, Foss PCD, Sullivan JO, Pelto R, Zeller M, Birge RR, Crundwell G. Origin of the bathochromically shifted optical spectra of meso-tetrathien-2- and 3-ylporphyrins as compared to meso-tetraphenylporphyrin Phys. Chem. Chem. Phys. 2006; 8:2402–2412.
60. Ono N, Miyagawa H, Ueta T, Ogawa T, Tani H. Synthesis of 3,4-diarylpyrroles and conversion into dodecaarylporphyrins; a new approach to porphyrins with altered redox potentials. J. Chem. Soc. Perkin Trans. 1998; 1:1595–1601.
61. Gupta I, Hung C-H, Ravikanth M. Synthesis and structural characterization of meso-thienyl core-modified porphyrins. Eur. J. Org. Chem. 2003:4392–4400.
62. Shi D-F, Wheelhouse RT. A novel, high-yielding synthesis of meso-substituted porphyrins via the direct arylation of porphine. Tetrahedron Lett. 2002; 43:9341–9342.
63. Bhyrappa P, Bhavana P. meso-Tetrathienylporphyrins: Electrochemical and axial ligation properties. Chem. Phys. Lett. 2001; 349:399–404.
64. Odobel F, Suresh S, Blart E, Nicolas Y, Quintard J-P, Janvier P, Le Questel J-Y, Illien B, Rondeau D, Richomme P, Häupl T, Wallin S, Hammarström L. Synthesis of oligothiophene-bridged bisporphyrins and study of the linkage dependence of the electronic coupling. Chem.–Eur. J. 2002; 8:3027–3046. [PubMed: 12489234]
65. Medforth CJ, Haddad RE, Muzzi CM, Dooley NR, Jaquinod L, Shyr DC, Nurco DJ, Olmstead MM, Smith KM, Ma J-G, Shelnutt JA. Unusual aryl-porphyrin rotational barriers in peripherally crowded porphyrins. Inorg. Chem. 2003; 42:2227–2241. [PubMed: 12665356]
66. Shimidzu T, Segawa H, Wu F, Nakayama N. Approaches to conducting polymer devices with nanostructures: Photoelectrochemical function of one-dimensional and two-dimensional porphyrin polymers with oligothienyl molecular wire. J. Photochem. Photobiol. A. 1995; 92:121–127.

67. Collis GE, Campbell WM, Officer DL, Burrell AK. The design and synthesis of porphyrin/oligothiophene hybrid monomers. Org. Biomol. Chem. 2005; 3:2075–2084. [PubMed: 15917892]
68. Vollmer MS, Würthner F, Effenberger F, Emele P, Meyer DU, Stümpfig T, Port H, Wolf HC. Anthyloligothienylporphyirns: Energy transfer and light-harvesting systems. Chem. Eur. J. 1998; 4:260–269.
69. Friedlein R, Kieseritzky F. v. Braun S, Linde C, Osikowicz W, Hellberg J, Salaneck WR. Solution-processed, highly-oriented supramolecular architectures of functionalized porphyrins with extended electronic states. Chem. Commun. 2005; 15:1974–1976.
70. Lau KSF, Zhao S, Ryppa C, Jockusch S, Turro NJ, Zeller M, Gouterman M, Khalil GE, Brückner C. Synthesis, structure, and optical Properties of the platinum(II) complexes of indaphyrin and thiaindaphyrin. Inorg. Chem. 2009; 48:4067–4074. [PubMed: 19341300]
71. You Y, Gibson SL, Hilf R, Ohulchanskyy TY, Detty MR. Core-modified porphyrins. Part 4: Steric effects on photophysical and biological properties in vitro. Bioorg. Med. Chem. 2005; 13:2235–2251. [PubMed: 15727875]
72. Li G, Bhosale S, Tao S, Guo R, Bhosale S, Li F, Zhang Y, Wang TY, Fuhrhop J-H. Very stable, highy electroactive polymers of zinc(II)-5,15-bisthienylphenyl porphyrin exhibiting charge-trapping effects. Polymer. 2005; 46:5299–5307.
73. Maruyama H, Segawa H, Sodota S, Sato T, Kosai N, Sagisaka S, Shimidzu T, Tanaka K. Electrochemical construction of ultrathin film composed of quasi two-dimensional poprhyrin polymers. Synth. Met. 1998; 96:141–149.
74. Chen W, Akhigbe J, Brückner C, Li CM, Lei Y. Electrocatalytic four-electron reduction of dioxygen by electrochemically depositedpoly{[meso-tetrakis(2-thienyl)porphyrinato]cobalt(II)}. J. Phys. Chem. C. 2010; 114:8633–8638.
75. Chen W, Ding Y, Akhigbe J, Brückner C, Li CM, Lei Y. Enhanced electrochemical oxygen reduction-based glucose sensing using glucose oxidase on nanodendritic poly[meso-tetrakis(2-thienyl)porphyrinato]cobalt(II)-SWNTs composite electrodes. Biosens. Bioelectron. 2010; 26:504–510. [PubMed: 20813516]
76. Chen W, Wang Y, Brückner C, Li CM, Lei Y. Poly[meso-tetrakis(2-thienyl)porphyrin] for the sensitive electrochemical detection of explosives. Sens. Actuators. B. 2010; 147:191–197.
77. Steene E, Wondimagegn T, Ghosh A. Electrochemical and electronic absorption spectroscopic studies of substituent effects in iron(IV) and manganese(IV) corroles. Do the compounds feature high-valent metal centers or noninnocent corrole ligands? Implications for peroxidase compound I and II intermediates. J. Phys. Chem. B. 2001; 105:11406–11413. (Correction/addition: J. Phys. Chem. B, 2002,106, 5312.)
78. Gryko DT, Piechota KE. Straightforward route to trans-A_2B-corroles bearing substituents with basic nitrogen atoms. J. Porphyrins Phtalocyanines. 2002; 6:81–97.
79. Gryko DT, Koszarna B. Refined methods for the synthesis of meso-substituted A_3- and trans-A_2B-corroles. Org. Biomol. Chem. 2003; 1:350–357. [PubMed: 12929430]
80. Maiti N, Lee J, Kwon SJ, Kwak J, Do Y, Churchill DG. Synthetic, crystallographic and electrochemical studies of thienyl-substituted corrole complexes of copper and cobalt. Polyhedron. 2006; 25:1519–1530.
81. Egorova OA, Tsay OG, Khatua S, Meka B, Maiti N, Kim M-K, Kwon SJ, Huh JO, Bucella D, Kang S-O, Kwak J, Churchill DG. Synthetic, cyclic voltammetric, structural, EPR, and UV-vis spectroscopic studies of thienyl-containing meso-A_2B-cor(Cr^V=O) systems: Consideration of three interrelated molecular detection modalities. Inorg. Chem. 2010; 49:502–512. [PubMed: 20017519]
82. Maiti N, Lee J, Do Y, Shin HS, Churchill DG. Synthesis and structures of thienyl-substituted 5-dipyrromethane isomers. J. Chem. Crystallogr. 2005; 35:949–955.
83. Egorova OA, Tsay OG, Khatua S, Huh JO, Churchill DG. A chiral meso-ABC-corrolatochromium(V) complex. Inorg. Chem. 2009; 48:4634–4636. [PubMed: 19371066]
84. Choi SH, Pang K, Kim K, Churchill DG. Cu^{2+} Colorimetric sensing and fluorescence enhancement and Hg^{2+} fluorescence diminution in “scorpionate”-like tetrathienyl-substituted boron-dipyrrins. Inorg. Chem. 2007; 46:10564–10577. [PubMed: 17990871]

85. Choi SH, Kim K, Jeon J, Meka B, Bucella D, Pang K, Khatua S, Lee J, Churchill DG. Optical effects of S-oxidation and Mn^{+} binding in meso-thienyl dipyrrin systems and of stepwise bromination of 4,4-difluoro-8-(2,5-dibromo-3-thienyl)-4-bora-3a,4a-diaza-s-indacene. Inorg. Chem. 2008; 47:11071–11083. [PubMed: 18986134]
86. Kim K, Jo C, Easwaramoorthi S, Sung J, Kim DH, Churchill DG. Crystallographic, photophysical, NMR spectroscopic and reactivity manifestations of the “8-heteroaryl Effect” in 4,4-difluoro-8-(C_4H_3X)-4-bora-3a,4a-diaza-s-indacene (X = O, S, Se) (BODIPY) Systems. Inorg. Chem. 2010; 49:4881–4894. [PubMed: 20420417]
87. Singh AP, Lee KM, Murale DP, Jun T, Liew H, Suh Y-H, Churchill DG. Novel sulphur-rich BODIPY systems that enable stepwise fluorescent O-atom turn-on and H_2O_2 neuronal system probing. Chem. Commun. 2012; 48:7298–7300.
88. Singh AP, Murale DP, Ha Y, Liew H, Lee KM, Segev A, Suh Y-H, Churchill DG. A novel, selective, and extremely responsive thienyl-based dual fluorogenic probe for tandem superoxide and Hg^{2+} chemosensing. Dalton Trans. 2013; 42:3285–3290. [PubMed: 23135623]
89. Singh AP, Tsay OG, Murale DP, Jun T, Liew H, Suh Y-H, Churchill DG. Extremely selective “turn-on” fluorescence detection of hypochlorite confirmed by proof-of-principle neurological studies via esterase action in living cells. Analyst. 2013; 138:2829–2832. [PubMed: 23571476]
90. Briñas RP, Brückner C. Triarylcorroles by oxidative coupling of triaryltetrapyrranes. Synlett. 2001; 3:442–444.
91. Becke AD. Density-functional thermochemistry. III. The role of exact exchange. J. Phys. Chem. 1993; 98:5648–5652.
92. Frisch, MJ.; Trucks, GW.; Schlegel, HB.; Scuseria, GE.; Robb, MA.; Cheeseman, JR.; Scalmani, G.; Barone, V.; Mennucci, B.; Petersson, GA.; Nakatsuji, H.; Caricato, M.; Li, X.; Hratchian, HP.; Izmaylov, AF.; Bloino, J.; Zheng, G.; Sonnenberg, JL.; Hada, M.; Ehara, M.; Kitao, O.; Nakai, H.; Vreven, T.; Montgomery, J.; J. A.; Peralta, JE.; Ogliaro, F.; Bearpark, M.; Heyd, JJ.; Brothers, E.; Kudin, KN.; Staroverov, VN.; Kobayashi, R.; Normand, J.; Raghavachari, K.; Rendell, A.; Burant, JC.; Iyengar, SS.; Tomasi, J.; Cossi, M.; Rega, N.; Millam, JM.; Klene, M.; Knox, JE.; Cross, JB.; Bakken, V.; Adamo, C.; Jaramillo, J.; Gomperts, R.; Stratmann, RE.; Yazyev, O.; Austin, AJ.; Cammi, R.; Pomelli, C.; Ochterski, JW.; Martin, RL.; Morokuma, K.; Zakrzewski, VG.; Voth, GA.; Salvador, P.; Dannenberg, JJ.; Dapprich, S.; Daniels, AD.; Farkas, O.; Foresman, JB.; Ortiz, JV.; Cioslowski, J.; Fox, DJ. Gaussian 09, Revision A.02. Gaussian, Inc.; Wallingford, CT.: 2009.
93. Barone V, Cossi M, Tomasi J. Geometry optimization of molecular structures in solution by the polarizable continuum model. J. Comput. Chem. 1998; 19:404–417.
94. Tomasi J, Mennucci B, Cammi R. Quantum mechanical continuum solvation models. Chem. Rev. 2005; 105:2999–3093. [PubMed: 16092826]
95. Clark T, Chandrasekhar J, Spitznagel GW, Schleyer PVR. Efficient diffuse function-augmented basis-sets for anion calculations. 3. The 3-21+G basis set for 1st-row elements, Li-F. J. Comp. Chem. 1983; 4:294–301.
96. Stanton JF, Bartlett RJ. Equation of motion coupled-cluster method: A systematic biorthogonal approach to molecular excitation energies, transition probabilities, and excited state properties. J. Chem. Phys. 1993; 98:7029–7039.
97. Koch H, Kobayashi R, Sánchez de Merás A, Jørgensen P. Calculation of size-intensive transition moments from the coupled cluster singles and doubles linear response function. J. Chem. Phys. 1994; 100:4393–4400.
98. Kállay M, Gauss J. Calculation of excited-state properties using general coupled-cluster and configuration-interaction models. J. Chem. Phys. 2004; 121:9257–9269. [PubMed: 15538846]
99. Nakatsuji H, Hirao K. Cluster expansion of the wavefunction. Symmetry-adapted-cluster expansion, its variational determination, and extension of open-shell orbital theory. J. Chem. Phys. 1978; 68:2053–2065.
100. Nakatsuji H. Cluster expansion of the wavefunction: Calculation of electron correlations in ground and excited states by SAC and SAC CI theories. Chem. Phys. Lett. 1979; 67:334–342.
101. Nakatsuji H. Description of two- and many-electron processes by the SAC-CI method Chem. Phys. Lett. 1991; 177:331–337.

102. Ishida M, Toyota K, Ehara M, Frisch MJ, Nakatsuji H. Analytical energy gradient of the symmetry-adapted-cluster configuration-interaction general-R method for singlet to septet ground and excited states. J. Chem. Phys. 2004; 120:2593–2605. [PubMed: 15268403]

103. Nakajima T, Nakatsuji H. Energy gradient method for the ground, excited, ionized, and electron-attached states calculated by the SAC (symmetry-adapted cluster)/SAC-CI (configuration interaction) method Chem. Phys. 1999; 242:177–193.

104. Dunning, TH., Jr.; Hay, PJ. Modern theoretical chemistry.. In: Schaefer, HF., editor. In Modern Theoretical Chemistry. Vol. 3. Plenum; New York, New York: 1976. p. 1-28.

105. Caricato M, Mennucci B, Scalmani G, Trucks GW, Frisch MJ. Electronic excitation energies in solution at equation of motion CCSD level within a specific polarizable continuum model approach. J. Chem. Phys. 2010; 132:0841021–0841027.

106. Wagner NL, Greco JA, Enriquez MM, Frank HA, Birge RR. The Nature of the intramolecular charge transfer state in peridinin. Biophys. J. 2013; 104:1314–1325. [PubMed: 23528091]

107. Enriquez MM, Hananoki S, Hasegawa S, Kajikawa T, Katsumura S, Wagner NL, Birge RR, Frank HA. Effect of molecular symmetry on the spectra and dynamics of the intramolecular charge transfer (ICT) state of peridinin. J. Phys. Chem. B. 2013; 116:10748–10756. [PubMed: 22889055]

108. Bhattacharya D, Singh P, Sarkar S. Synthesis, X-structure and solvent induced electronic states tuning of meso-tris(4-nitrophenyl)corrolato-copper complex. Inorg. Chim. Acta. 2010; 363:4313–4318.

109. Palmer JH, Durrell AC, Gross Z, Winkler JR, Gray HB. Near-IR phosphorescence of iridium(III) corroles at ambient temperature. J. Am. Chem. Soc. 2010; 132:9230–9231. [PubMed: 20568752]

111. Shen J, Shao J, Ou Z, Koszarna WE,B, Gryko DT, Kadish KM. Electrochemistry and spectroelectrochemistry of meso-substituted free-base corroles in nonaqueous media: Reactions of $(Cor)H_3$, $[(Cor)H_4]^+$, and $[(Cor)H_2]^-$. Inorg. Chem. 2006; 45:2251–2265. [PubMed: 16499391]

112. Ding T, Harvey JD, Ziegler CJ. N-H tautomerization in triaryl corroles. J. Porphyrins Phthalocyanines. 2005; 9:22–27. (see also erratum in Ding, T.; J. D. Harvey and C. J. Ziegler (2005) J. Porphyrins Phthalocyanines 9, 528.)

113. Fleischer EB. The Structure of Porphyrins and Metalloporphyrins. Acc. Chem. Res. 1970; 3:105–112.

114. Hashimoto T, Choe Y-K, Nakano H, Hirao K. Theoretical study of the Q and B bands of free-base, magnesium, and zinc porphyrins, and their derivatives. J. Phys. Chem. A. 1999; 103:1894–1904.

115. Gouterman M. Spectra of porphyrins. J. Mol. Spectrosc. 1961; 6:138–163.

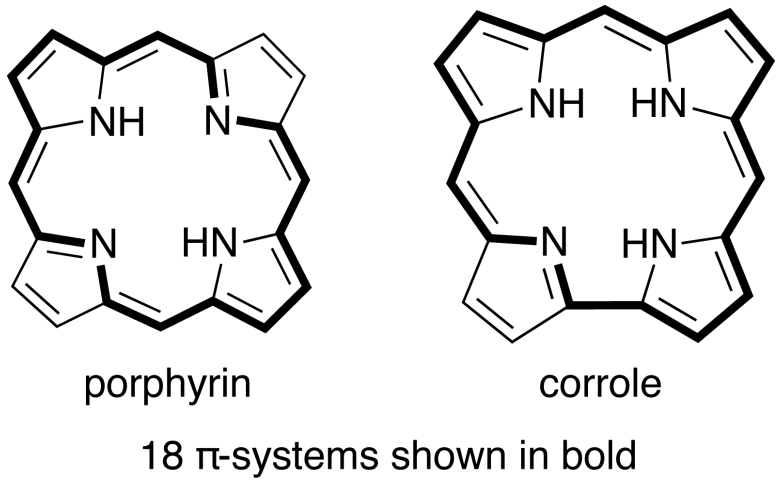

Scheme 1.
Framework structures of corroles and porphyrins.

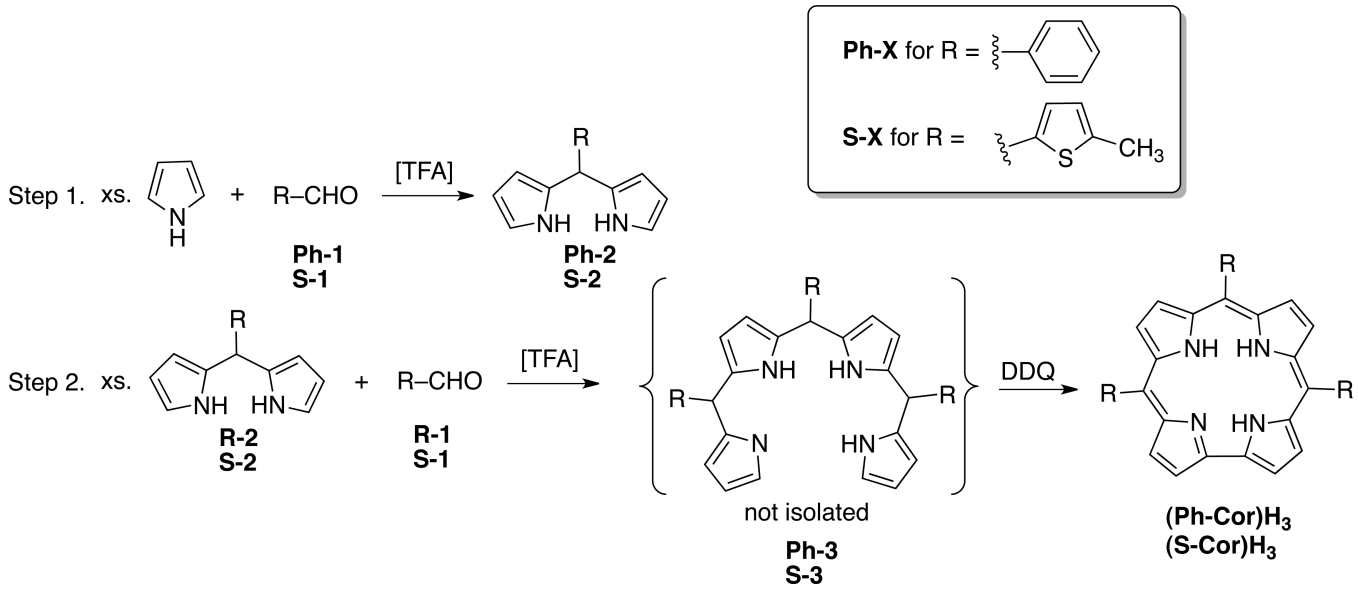

Scheme 2.
Synthesis of the triarylcorroles investigated.

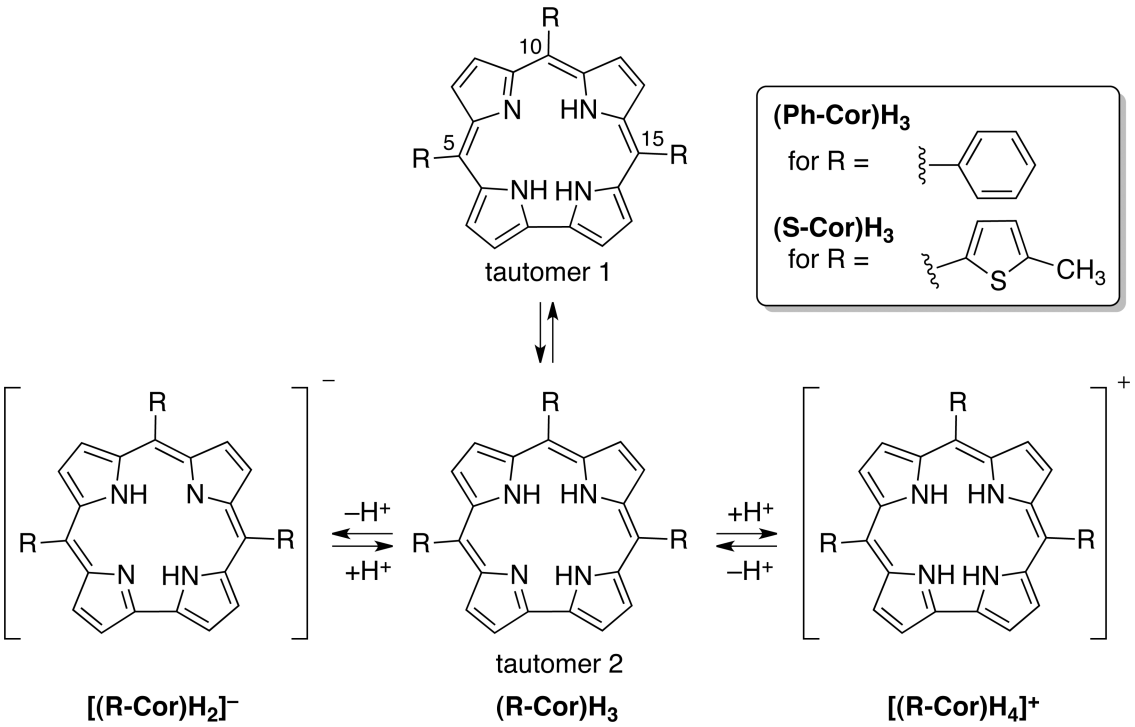

Scheme 3.

Tautomers and protonation states of the triarylcorroles investigated.

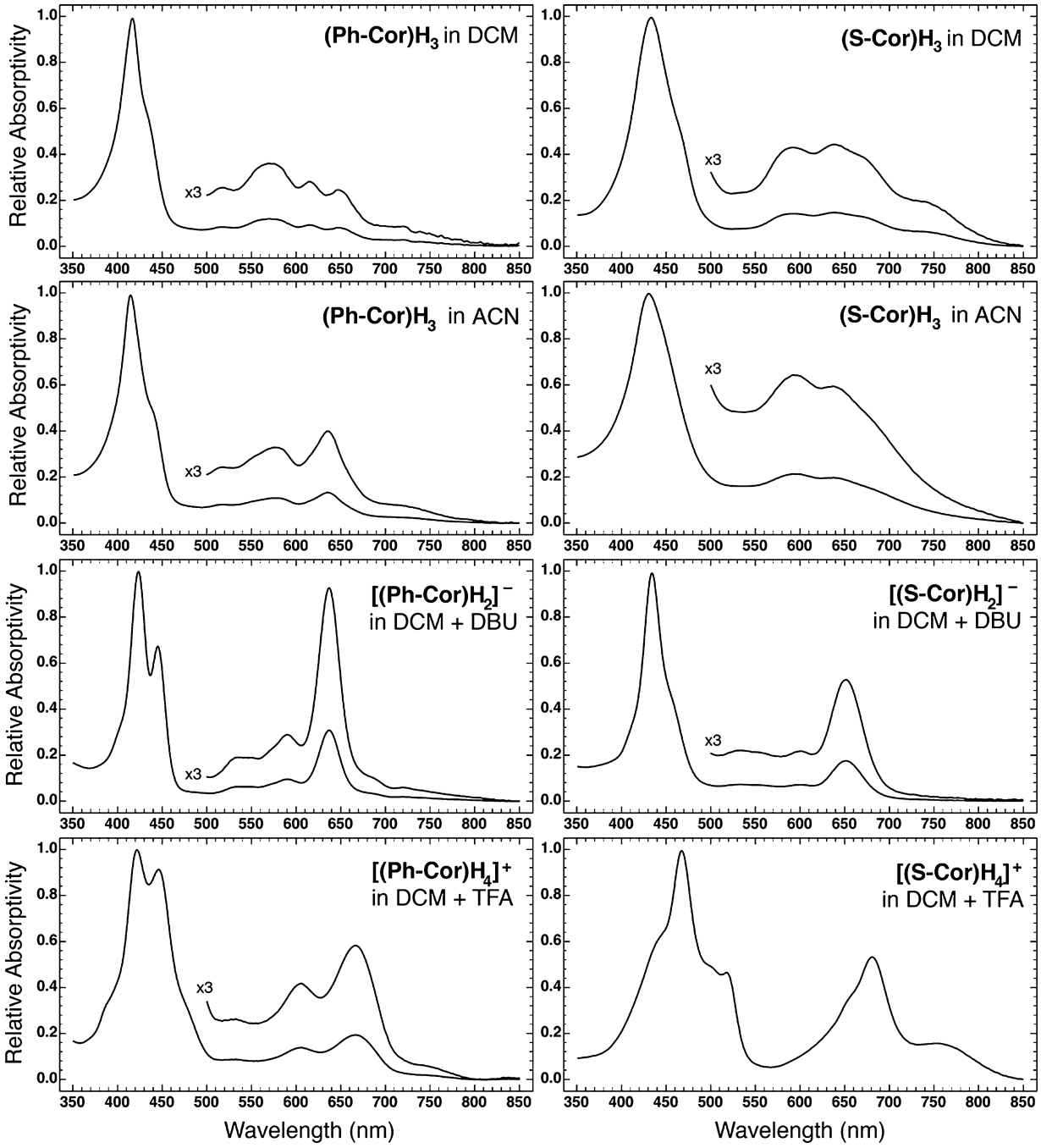

Figure 1.

Experimental absorption spectra of **(Ph-Cor)H_3** and **(S-Cor)H_3** in the solvents indicated. All spectra are normalized to the absorption maximum of the Soret band.

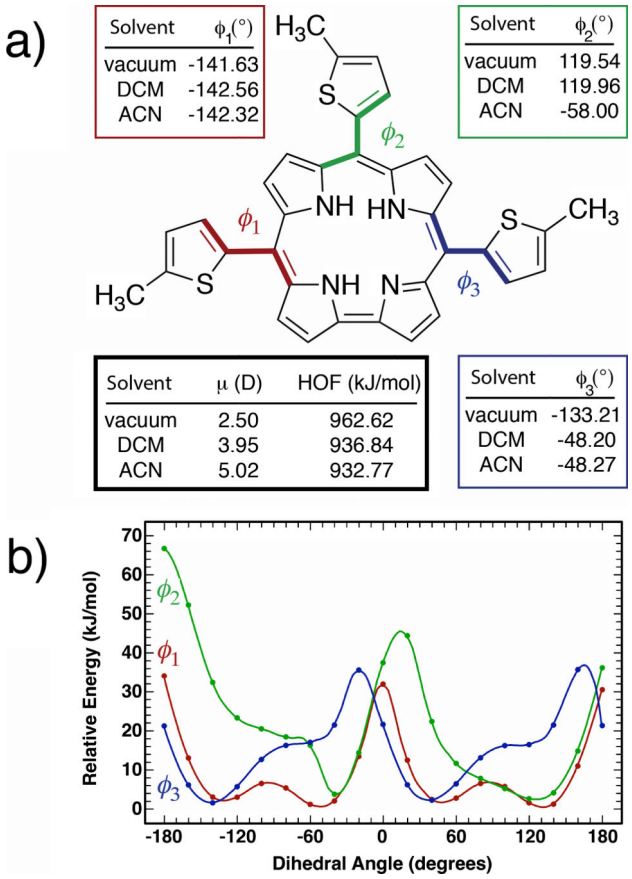

Figure 2.

Potential energy surface (PES) scans were performed for the three thienyl groups of **(S-Cor)H_3** to determine a global minimum of the structure. The resulting minima in vacuum, DCM, and ACN are presented in (A). The curves presented in (B) provide an example of the PES of groups 1 (red), 2 (green), and 3 (blue). See text for further details regarding the high variability of energetics due to inherent asymmetry

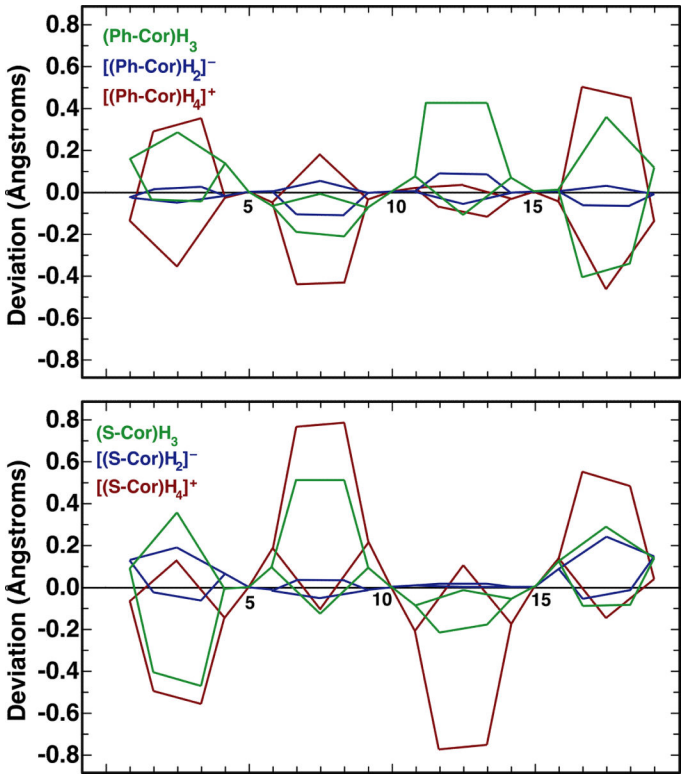

Figure 3.

A linear display of the deviation of the 23 macrocycle framework atoms. For the assignment of the 5, 10, and 15 positions, see Scheme 3. These three *meso*-carbon atoms served to define the zero-point plane against which the relative deviation were plotted.

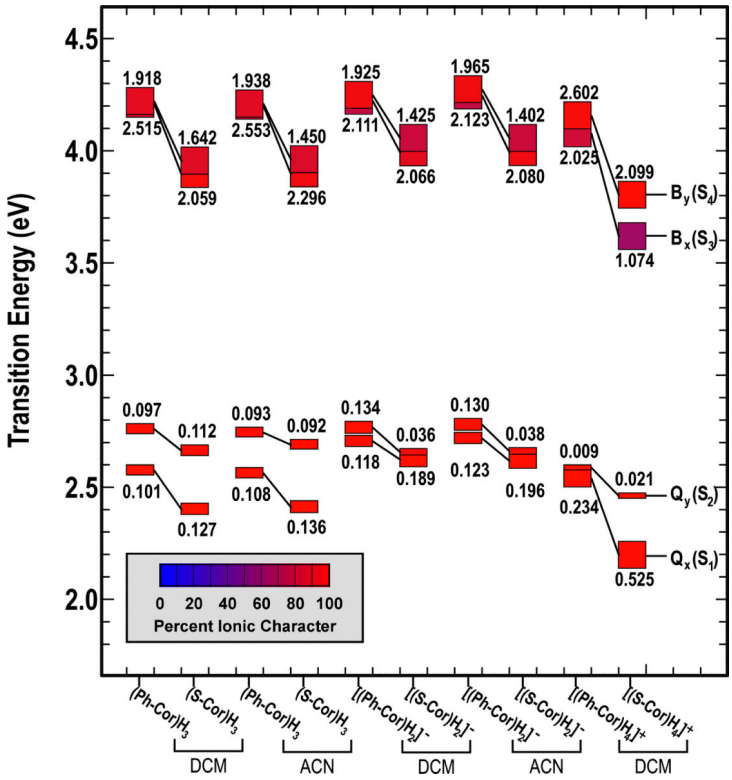

Figure 4.

Excited singlet state level ordering of the first 4 excited states of **(Ph-Cor)H_3** and **(S-Cor)H_3** in the neutral, anionic, and cationic states, in DCM and ACN, as calculated using EOM CCSD methods. The oscillator strengths are given directly above or below each state rectangle, and the thickness of the rectangles are proportional to this value. The ionic versus covalent character of each state follows the colorimetric scheme shown at the lower left.

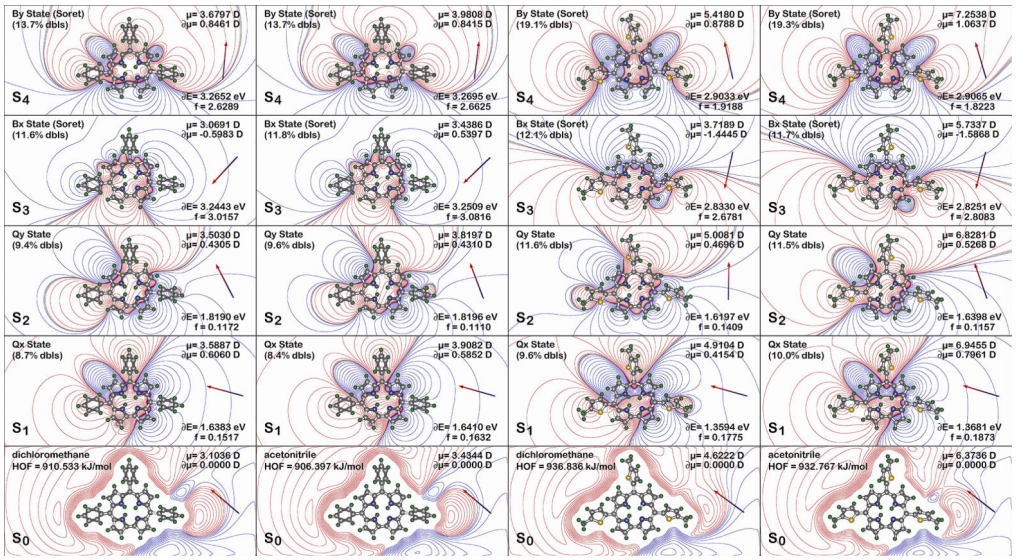

Figure 5.

Electrostatic properties of the ground state (S_0) and the charge shifts induced by excitation into the first four excited singlet states for **(Ph-Cor)H_3** and **(S-Cor)H_3** in DCM and in ACN based on SAC-CI methods. The two left panels and the two right panels illustrate **(Ph-Cor)H_3** and **(S-Cor)H_3**, respectively, with the solvents labeled within each panel. The ground state contours display the approximate electrostatic field surrounding the molecule where red contours indicate regions of excess positive charge and blue contours indicate regions of excess negative charge. The contours associated with the excited states (S_1, S_2, S_3 and S_4) represent the shift in charge induced by excitation into these states where red contours indicate increased positive charge and blue contours indicate increased negative charge following excitation. The arrows display the dipole moment direction, and the transition energies (δE in electron volts relative to uncorrelated ground state), oscillator strengths (f) and dipole moments (μ in Debye) are shown at the upper right of each panel. The contribution of doubly excited configurations (dbls) is shown as a percentage at upper left of each excited state.

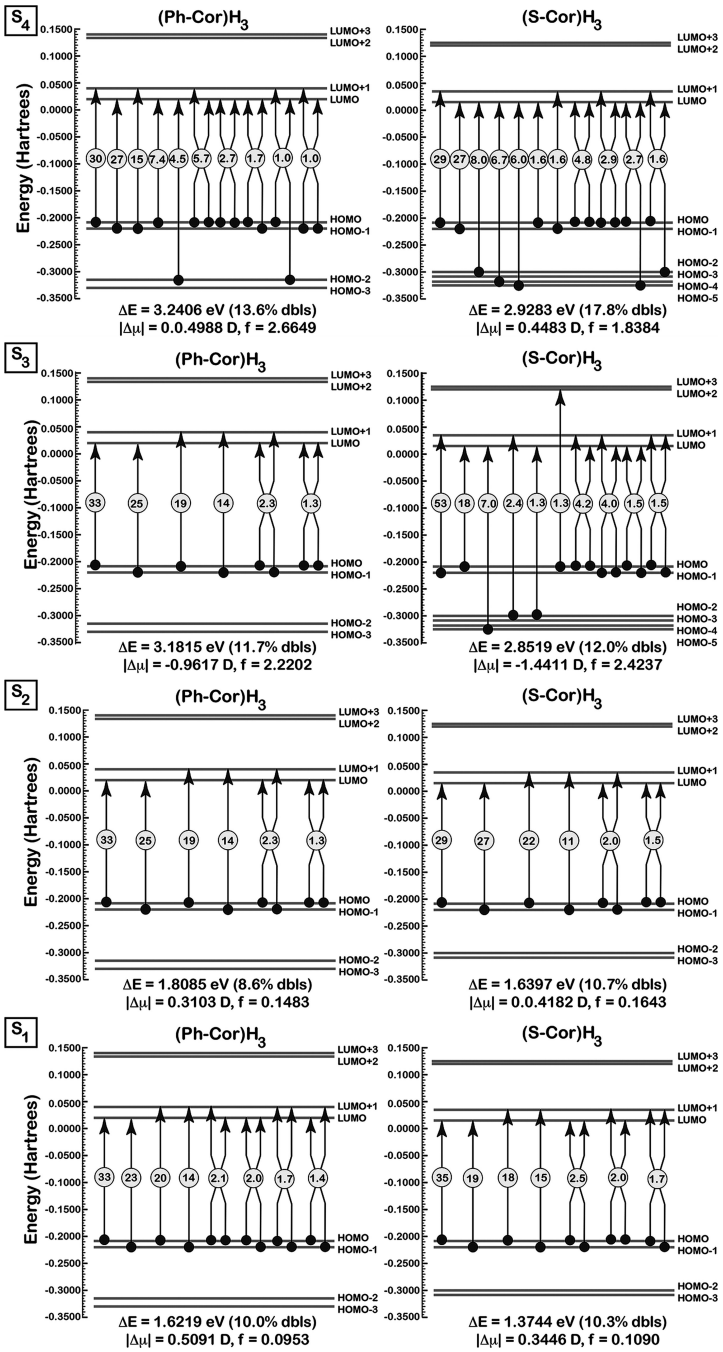

Figure 6.

Configurational analysis of the four lowest-lying excited singlet states of **(Ph-Cor)H_3** and **(S-Cor)H_3** based on SAC-CI molecular orbital theory. Each excited state is described as a linear combination of single or double excitations, with the percent contribution of each configuration shown in the circles. Only configurations contributing 1% or more are shown. Doubly excited configurations have two source (circles) and destination (arrows) symbols.

Table 1

Heat of formation (HOF, kJ/mol) for ground state geometry optimizations of the neutral, mono-anionic, and mono-cationic forms of (Ph-Cor)H_3 and (S-Cor)H_3.

	Solvent		
Compound	**Vacuum**	**DCM**	**ACN**
(Ph-Cor)H_3	1043.09	910.53	906.40
(S-Cor)H_3	962.62	936.84	932.77
[(Ph-Cor)H2]$^-$	614.32	459.92	492.56
[(S-Cor)H_2]$^-$	649.87	436.62	470.81
[(Ph-Cor)H_4]$^+$	1534.57	1403.20	Not determined[a]
[(S-Cor)H_4]$^+$	1427.81	1301.25	Not determined[a]

[a]The mono-cationic structures were not determined in ACN because the configurations were irrelevant to the experimental data.

Table 2

Dihedral angles for the lowest energy ground state geometries of the neutral (DCM), mono-anionic (ACN), and mono-cationic (DCM) forms of (Ph-Cor)H_3 and (S-Cor)H_3.

	Dihedral Angles		
Compound	φ_1(○)	φ_2(○)	φ_3(○)
(Ph-Cor)H_3	135.66	−118.20	53.17
(S-Cor)H_3	−141.63	119.54	−48.98
[(Ph-Cor)H_2]$^-$	127.32	63.32	−53.23
[(S-Cor)H_2]$^-$	127.30	101.90	50.97
[(Ph-Cor)H_4]$^+$	136.41	66.87	45.41
[(S-Cor)H_4]$^+$	−143.89	−43.40	37.70